ACS APPLIED MATERIALS & INTERFACES

www.acsami.org

Research Article

In Vitro Development of Human iPSC-Derived Functional Neuronal Networks on Laser-Fabricated 3D Scaffolds

Anastasia Koroleva,*,△ Andrea Deiwick,△ Ayman El-Tamer, Lothar Koch, Yichen Shi, Estefanía Estévez-Priego, Adriaan-Alexander Ludl, Jordi Soriano, Daria Guseva, Evgeni Ponimaskin, and Boris Chichkov

Cite This: *ACS Appl. Mater. Interfaces* 2021, 13, 7839–7853

Read Online

ACCESS | Metrics & More | Article Recommendations | Supporting Information

ABSTRACT: Neural progenitor cells generated from human induced pluripotent stem cells (hiPSCs) are the forefront of "brain-on-chip" investigations. Viable and functional hiPSC-derived neuronal networks are shaping powerful *in vitro* models for evaluating the normal and abnormal formation of cortical circuits, understanding the underlying disease mechanisms, and investigating the response to drugs. They therefore represent a desirable instrument for both the scientific community and the pharmacological industry. However, culture conditions required for the full functional maturation of individual neurons and networks are still unidentified. It has been recognized that three-dimensional (3D) culture conditions can better emulate *in vivo* neuronal tissue development compared to 2D cultures and thus provide a more desirable *in vitro* approach. In this paper, we present the design and implementation of a 3D scaffold platform that supports and promotes intricate neuronal network development. 3D scaffolds were produced through direct laser writing by two-photon polymerization (2PP), a high-resolution 3D laser microstructuring technology, using the biocompatible and nondegradable photoreactive resin Dental LT Clear (DClear). Neurons developed and interconnected on a 3D environment shaped by vertically stacked scaffold layers. The developed networks could support different cell types. Starting at the day 50 of 3D culture, neuronal progenitor cells could develop into cortical projection neurons (CNPs) of all six layers, different types of inhibitory neurons, and glia. Additionally and in contrast to 2D conditions, 3D scaffolds supported the long-term culturing of neuronal networks over the course of 120 days. Network health and functionality were probed through calcium imaging, which revealed a strong spontaneous neuronal activity that combined individual and collective events. Taken together, our results highlight advanced microstructured 3D scaffolds as a reliable platform for the 3D *in vitro* modeling of neuronal functions.

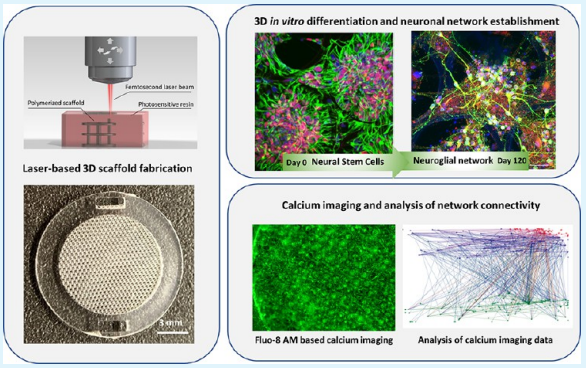

KEYWORDS: *3D neuronal culture, human neural stem cells, scaffold, two-photon polymerization, Ca imaging, NETCAL analysis*

INTRODUCTION

The goal of most current tissue models, including neuronal tissue, is to establish systems that can be used to study pharmacology, network formation, pathology, or any combination thereof.[1] Thus, the *in vitro* creation of neuronal networks in 3D environments represents a challenging and highly important task for basic research in the field of central nervous system (CNS) development and function, identification of pathological hallmarks, as well as drug discovery for the treatment of neurological and neurodegenerative diseases.[2,3] Studies of the development and function of the diseased and healthy human cerebral cortex have been often limited by a lack of proper cell model systems. Indeed, primary human neuronal cultures are difficult to access, and much of our knowledge about brain plasticity has been gained through the use of animal *in vitro* and *in vivo* models. A number of approaches to develop *in vitro* neural tissue models using primary rodent neuronal cultures have been undertaken.[4−6] Although animal studies still play a significant role in the understanding of brain development and function, the translation of these findings into human conditions or medical treatments is difficult and challenging.

The successes in stem cell biology are generally predicted to hold a great potential for the study and development of treatments of neurodegenerative diseases.[7,8] Recent developments in the reprogramming of human adult somatic cells

Received: October 13, 2020
Accepted: January 13, 2021
Published: February 9, 2021

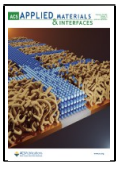

(e.g., fibroblasts from individual patients) into pluripotent stem cells (iPSCs) enabled the establishment of patient-specific stem cells.[9] These pluripotent cells can be exponentially expanded and, under appropriate conditions, can be directed to differentiate into specific cell types, including neurons. Thus, the iPSC-derived human cerebral neocortical neural stem cells (NSCs), and neurons developed from them, have facilitated the study of the molecular mechanisms regulating cortical development and plasticity in humans as well as their malfunctions.

To date, most *in vitro* studies in the field of neuroscience are performed using 2D cultures. However, 2D neuronal cultures cannot properly mimic the complexity of coordinated 3D interactions of *in vivo* brain neuronal networks. A 3D environment provides a larger surface area for cell accommodation, distribution, and growth. It has been demonstrated that 2D neuronal cultures exhibit electrical responses different to those in 3D conditions, which support the fact that neuronal cells in a 3D environment form more cell-to-cell connections.[10] Thus, *in vitro* models utilizing iPSC-derived neuronal cells in 3D culture conditions would represent a more adequate *in vivo* like environment as compared to 2D cultures.

Various approaches for creating *in vitro* neural 3D cultures from reaggregated cells have been developed, including the highly popular hydrogel 3D cultures,[11−14] cellular spheroid cultures,[2] and scaffold-based 3D cultures.[15,16] The so-called spheroid (or organoid)-based 3D neuronal cultures are of widespread use in many research laboratories and do not require special expensive equipment. However, although neural 3D cultures based on spheroids can recapitulate some aspects of 3D cell morphology, important cell-to-cell and cell-to-substrate/matrix interactions are spatially limited in the cell spheroid system.

3D neural cultures, where cells are grown through a porous synthetic scaffold or a hydrogel-based matrix, represent more desired 3D culture models. Such *engineered* neuronal models can better succeed in controlling the organization and composition of the cellular microenvironment. Application of materials with desired biological or structural properties, such as soft hydrogels or stiff polymeric platforms, is one of the ways in which 3D neuronal *in vitro* models can be constructed in a controlled and consistent manner. Several studies have been devoted to the development of *in vitro* 3D neuronal systems using porous polymeric scaffolds, hydrogels, and the combination thereof. Lam et al. have systematically evaluated the cell seeding and culture conditions for the creation of 3D *in vitro* neuronal cultures using ECM−collagen hydrogels. They found that the increased cell concentration caused their heterogeneous spatial distribution in 3D and was proportional to the rise in cell death. Hence, the studied ECM−collagen 3D cultures could only be maintained for 30 days.[17] On the other hand, Dingle et al. used a silk−collagen composite scaffold to study the development of primary cortical cultures in a 3D environment along 3 weeks. They showed that the neuronal network exhibited rich functional traits, and explored different pharmacological perturbations to demonstrate the responsiveness of the network.[1] In their recent works, the group of D. Kaplan has applied silk fibroin scaffolds and collagen hydrogel for the creation of a brainlike neural tissue platform using primary rat cortical neurons and human iPSCs.[18,19] The proposed silk donut-shaped scaffold filled with a collagen hydrogel emulates the interface of ″gray″ and ″white″ brain matter and supported the *in vitro* culture of functional iPSC-derived neuronal networks for up to 2 years.[19] Even though the fabrication of the silk fibroin donut-shaped scaffold does not require expensive equipment, its inner porous architecture represents the sponge with a heterogeneous mesh of small and large pores. Such a heterogeneous scaffold architecture can result in poor pore interconnectivity and prevent the outgrowth of long neuronal neurites.

Truly 3D polymeric scaffold platforms with a complex and predictable architecture represent a powerful tool in developing an instructive milieu for the *in vitro* cell accommodation and development of tissues with certain functional properties. However, the reproducible fabrication of such 3D scaffold platforms with a regular architectural microstructure is not an easy task. Rapidly advancing 3D prototyping technologies, including bioprinting and direct laser fabrication methods, are very promising for the fabrication of 3D scaffold platforms for the development of spatially distributed neuronal cultures *in vitro*. These technologies allow a precise and reproducible 3D scaffold fabrication according to specific culture needs. The highest level of flexibility and reproducibility in terms of structural design can be achieved using the two-photon polymerization technique (2PP).[15,20−22] The 2PP 3D microstructuring method uses the simultaneous absorption of two photons of near-infrared (at 780 nm) or green (515 nm) laser light, which takes place at high laser intensity within a spatially localized focus region. This process occurs in a volume of photosensitive liquid material. During microstructuring, both the focus and sample positions can be computer controlled using focusing optics with integrated scanner and piezoelectric translational axes. This enables practically unlimited possibilities for 3D microstructuring and allows the fabrication of scaffolds with a complex inner microarchitecture.

Our previous studies involved the application of laser microstructured scaffolds from a number of materials for various tissue-engineering applications. We produced the scaffolds from a Zr−Si-based inorganic−organic hybrid material and from different types of polylactic acid (PLA) for bone tissue modeling using human mesenchymal stromal cells.[23−25] It was previously shown that Zr−Si-based scaffolds provide a good artificially fabricated platform for the effective adherence of dissociated mice hippocampal neuronal cells and are suitable for the creation of 3D neural network models.[26] The potential of laser-fabricated scaffold matrices from biodegradable chitosan and chitosan−hyaluronic acid complex for neurotransplantation has also been proved.[27,28]

The aim of the present study is to establish a reproducible human iPSC-derived neuronal 3D *in vitro* model using an advanced 2PP laser technique for the fabrication of a 3D scaffold platform. Since biocompatibility is an essential requirement for the development of cell cultures embedded in 3D scaffolds, we used the biocompatible resin DClear—a mixture of methacrylic acid esters and a photoinitiator[29]—to produce 3D scaffolds for the establishment of viable and long-term stable 3D neuronal cultures. Laser-fabricated scaffolds were seeded with human iPSC-derived neural stem cells (NSCs), which were allowed to differentiate over the course of 120 days. The NSCs express typical markers of cerebral cortical neural stem and progenitor cells such as PAX6, FOXG1, and Nestin and spontaneously form polarized neural tubelike rosette structures when plated as a monolayer in culture. Additionally, NSCs are capable of generating a spectrum of cerebral cortical excitatory and inhibitory neurons that are electrically active and have the ability to form

https://dx.doi.org/10.1021/acsami.0c16616
ACS Appl. Mater. Interfaces 2021, 13, 7839−7853

functional synapses and circuits *in vitro*.[7,48] We investigated the ability of NSCs, grown and differentiated on these 3D scaffolds, to develop mature and functional neuronal networks. With this culture system, we demonstrate that 3D microstructured scaffolds can dictate several important characteristics of NSC-derived neuronal networks that include (1) proper 3D cell accommodation, long-term survival, and 3D network formation; (2) *in vitro* functional maturation of the neuronal network (synaptogenesis) and spontaneous electrical activity; and (3) differentiation into specific cortical neuronal phenotypes and glia.

MATERIALS AND METHODS

Fabrication of 3D Scaffolds. 3D scaffolds were fabricated from the commercially available biocompatible resin DClear (Formlabs, Berlin, Germany).[30] The scaffolds were produced by the two-photon polymerization (2PP) method using a Ti:sapphire femtosecond laser system (Chameleon, Coherent, Germany) and 20× focusing objective (Zeiss Epiplan ×20, NA: 0.4).[23] Fabrication occurred at a 120 mm/s scanning speed and 100 mW laser power using a custom-written computer code to produce desired geometries from user-defined fabrication parameters. During the layer-by-layer fabrication approach, the next scaffold layer was produced by translating the stage with the sample 80 μm downward, and each next layer of the cylinder array was also shifted relative the center position of the previous layer by the half of the cylinder diameter (x and y shift). The layer-by-layer fabrication of cylinder arrays allowed the creation of a complex porous 3D scaffold structure (*honeycomb*) with increased available inner surface for neuronal cell attachment and network formation (Figure S1).

To prevent the lateral deformation (shrinkage) of thin scaffolds and to enable a more accurate scaffold handling, the scaffold structures were additionally embedded into a 1 mm wide ring frame from the same DClear resin. This was performed immediately after the 2PP scaffold fabrication by applying a mask projection lithography. After that, the 3D scaffolds were developed in 2-propanol to remove the unpolymerized material, washed twice in a fresh 2-propanol, and post-cured by a UV lamp.

2D polymer pellets with diameters of 10 mm and a thickness of approximately 800 μm were prepared from the DClear material by photopolymerization with ultraviolet (UV) light. For this purpose, multiwell chambered coverslips (Grace Bio-Labs, OR, USA) were filled with a liquid DClear monomer and subsequently cured using UV light (254 nm, dose 24 J cm^{-2}) to form pellets.

Cell Culture and Scaffold Seeding Procedure. Unless otherwise noted, cell culture media and supplements were purchased from Fisher Scientific GmbH (Schwerte, Germany). Cell culture plates were obtained from TPP-Techno Plastic Products AG (Trasadingen, Switzerland). Chemicals were purchased from Sigma-Aldrich (Deisenhofen, Germany). Human male iPSC-derived neuronal stem cells (NSCs) were provided by Axol Biosciences (ax0011; Cambridge, UK).

Cryopreserved NSCs were thawed and cultured according to supplier instructions. Briefly, NSCs were plated onto SureBond (Axol Biosciences)-coated six-well plates at a density of 5×10^4 cells/cm^2 in the Neural Plating-XF Medium (Axol Biosciences) and cultured in a humidified incubator with 5% CO_2 at 37 °C. The day after plating, the medium was replaced with an expansion medium consisting of KnockOut DMEM/F-12 supplemented with 1% Glutamax, 2% StemPro Neural Supplement, epidermal growth factor (EGF, 20 ng/mL; Axol Bioscience), basic fibroblast growth factor (bFGF, 20 ng/mL; Axol Bioscience), and 50 μg/mL gentamycin. At a confluence of 80−90%, the NSCs were split by using Accutase for 5 min at 37 °C. Human NSCs were seeded at a density of 5×10^4 cells/cm^2 and cultured onto Geltrex-ESC-coated culture vessels in the expansion medium during the initial plating supplemented with 1% RevitaCell, a modified Rho-kinase inhibitor. The medium was replaced with the expansion medium without RevitaCell after 24 h. NSCs were maintained in the expansion medium with two medium changes per week. For all cell experiments, NSCs of passages 2−5 were applied.

2PP fabricated 3D scaffolds and flat 2D pellets were placed in a 24-well plate in PBS and sterilized under UV light for 30 min before protein coating. After sterilization, the samples were coated with 1.0 mL of GIBCO rhLaminin-521 (2 μg/mL) and Geltrex-ESC (1:50 diluted in PBS) overnight at 37 °C. Before cell seeding, the samples were washed twice with sterile PBS and transferred into a new 24-well plate. Each sample was seeded with 1×10^5 NSCs suspended in 100 μL of the expansion medium supplemented with 1% RevitaCell and incubated for 2 h at 37 °C to allow initial cell attachment; thereafter, 1 mL of the medium was added per well. After 24 h, the medium was replaced with the expansion medium without RevitaCell. After 4 more days, the medium was changed into the neural induction medium consisting of the Neurobasal medium supplemented with a 2% B27 Serum-Free solution, 1% Glutamax, 200 μM ascorbic acid-2-phosphate, and 50 μg/mL gentamycin. Cells were cultured for up to 120 days and fed every second day by replacing half of the culture medium.

Immunocytochemistry. The immunofluorescence staining of the cell-seeded scaffolds was performed by a two-step indirect method. The samples were fixed in 4% paraformaldehyde for 1 h and permeabilized with 0.5% Triton X-100/PBS. Nonspecific antibody binding was inhibited by applying a 2% bovine serum albumin/PBS solution for 2 h at 37 °C. After blocking, the samples were incubated with primary antibodies (see Table S2 for details) optimally diluted in 0.5% Triton X-100/PBS overnight at 4 °C. After several washing steps, the samples were incubated with a fluorescence-conjugated secondary antibody at an appropriate dilution (see Table S2 for details) for 2 h at 37 °C. Cell nuclei were stained with Hoechst 33342. Scaffold samples were washed three times and stored in PBS prior to confocal microscopy (Inverted Confocal LSM Zeiss 780). Laser scanning microscopy (LSM) confocal imaging of 3D neuronal cultures was performed in depth to 120 μm beneath the sample surface depending on the neuronal network density.

Scanning Electron Microscopy Imaging. For scanning electron microscopy analysis, scaffolds with cells were fixed with 2.5% glutaraldehyde for 20 min followed by 2% osmium tetroxide for 30 min. After a number of washing steps and dehydration series with different increasing ethanol concentrations, the scaffolds were treated with hexamethyldisilazane. The scaffolds were then air-dried and subsequently sputter-coated with 100 nm of gold. SEM imaging was performed with a Quanta 400F microscope (FEI Company, OR, USA).

RNA Extraction and RT-PCR. RNA was extracted from cell cultures using the TriPure isolation reagent according to the manufacturer's protocol. For reverse transcription, 2 μg of DNAse-treated RNA was transcribed into cDNA using the Invitrogen SuperScript II Reverse Transcriptase Kit (Fisher Scientific GmbH, Schwerte, Germany). Polymerase chain reaction (PCR) amplification was performed in a peqSTAR thermocycler (PEQLAB Biotechnologie GMBH, Erlangen, Germany) using gene-specific primers (Eurofins MWG Operon, Ebersberg, Germany; primer sequences are presented in Table S1) and the Taq polymerase (Qiagen, Hilden, Germany). The various cDNA samples were adjusted to equal input concentrations by the expression level of the housekeeping gene GAPDH.

Western Blot Analysis. Total protein was isolated from cell monolayers and scaffold cultures with an ice-cold RIPA lysis buffer containing protease and phosphatase inhibitors (25 mM Tris−HCl (pH 7.6), 150 mM NaCl, 1% Nonidet P-40, 0.1% SDS, and 1% sodium deoxycholate) by sonication. The protein concentration of the lysate was quantified using a BCA protein assay (Roth, Karlsruhe, Germany). Ten micrograms of the protein extract was then loaded per lane on a 10% polyacrylamide resolving gel and separated by SDS-PAGE. After electrophoresis, proteins were transferred to a polyvinylidene fluoride (PVDF) membrane (Roth) by wet blotting using 20% methanol in Tris−glycine buffer. The membrane was blocked for 1 h in a 5% nonfat milk solution in Tris-buffered saline with 0.1% Tween (TBST) before incubation with primary antibodies

https://dx.doi.org/10.1021/acsami.0c16616
ACS Appl. Mater. Interfaces 2021, 13, 7839−7853

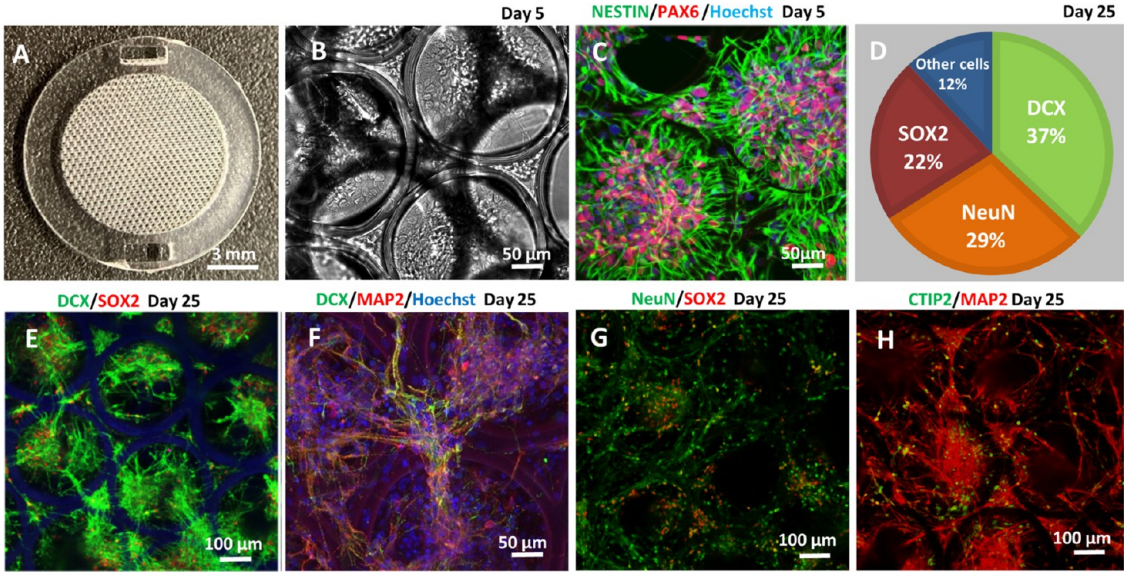

Figure 1. Generation of a 3D neuronal cell culture using laser-fabricated scaffolds. (a) General view of the scaffold structure ("honeycomb") used for 3D neuronal culture development. (b) Phase-contrast image showing uniformly distributed cells within the scaffold 5 days after seeding. (c) Immunofluorescence image depicting well-accommodated NSCs in the pores of the scaffold. The labeled proteins are Nestin and PAX6, characteristic of cortical stem cells. (d) Quantitative ratio of young (DCX+) and mature (NeuN+) neurons as well as SOX2+ multipotent neural progenitor cells in the scaffold at day 25 of culture/differentiation. (e–g) Expression of young and mature neuronal markers DCX/MAP2/NeuN and SOX2, indicating a healthy formation of a neuronal network. (h) Differentiation of early-born CTIP2+ cortical neurons from neural stem cells.

(for details see Table S2) overnight at 4 °C. After washing, the membrane was incubated with a horseradish peroxidase conjugated secondary antibody for 1 h at room temperature. Detection of the secondary antibody was performed with an enhanced chemiluminescence system using the Thermo Scientific SuperSignal West Femto Substrate.

Ca^{2+} Imaging and Analysis. Cell cultures were incubated with the calcium-sensitive dye Fluo-8 AM ester (10 μM, Biomol, Hamburg, Germany) in a neural differentiation medium at 37 °C for 1 h. Following dye loading, the cultures were rinsed thrice with a prewarmed external medium (EM) consisting of 10 mM Hepes, 130 mM NaCl, 4 mM KCl, 1 mM $MgCl_2$, 2 mM $CaCl_2$, 45 mM sucrose, and 10 mM glucose. Spontaneous calcium activity was acquired upon an AxioImager A1 microscope equipped with an AxioCm ICc1 camera and AxioVision software (version 4.8). Recorded data were analyzed using NETCAL (www.itscnetcal.com), a Matlab-run software package for the large-scale analysis of calcium imaging experiments in neuronal cultures.[31,32] Image sequences of spontaneous activity recordings (of jpeg format) were converted to TIF using the bioformats plugin of Fiji.[33] The main steps of the data analysis pipeline were the following: preprocessing, regions of interest (ROIs) identification, trace extraction, selection of active traces, spike inference, and network inference. They are described below. The preprocessing module calculated the average image and other general properties of the recording. Then, a Python script was used to detect cell bodies (soma) using the blob-detection algorithm of scikit-image.[34] Parameters were adjusted manually for each sample to optimize the number of cell bodies detected. Next, NETCAL extracted the traces for the selected ROIs. A trace fixer was used to correct for jumps and drifts in the fluorescence signal due to fluctuations in the fluorescence arc lamp, and the signal F_i of each ROI i was finally expressed in terms of the relative fluorescence increase as $X_i(\%) \equiv 100 \cdot (\Delta F/F_0)_i = (F_i - F_{i,0})/F_{i,0}$, where $F_{i,0}$ is the basal fluorescence of the ROI.

Active traces were then selected in NETCAL using a simple criterion based on the maximum amplitude and variability of the trace to distinguish spiking neurons from the noisy background. An ROI i was retained as active when its fluorescence signal amplitude verified $A_i \geq \beta A_{\text{average}}$, where β is a parameter in the range [0, 10], which was maintained fixed for all neurons in a given recording; $A_i = \max(X_i) - \min(X_i)$ is the maximum amplitude of the signal, and A_{average} is its average value.

The retained ROIs were ascribed as neurons. Their activations (spikes) were inferred using the OASIS algorithm with standard parameters, therefore transforming the set of fluorescence traces into times series.[35] For each network, the functional connectivity was computed using an algorithm based on transfer entropy implemented in NETCAL. Transfer entropy (TE) measures the amount of information transferred from Y to X.[36] This measure is nonlinear and nonsymmetric in Y and X and therefore captures the directionality of the interaction. We used the extended generalized transfer entropy (GTE) that accounts for the conditioning of the fluorescence signal.[37,38] The functional analysis provided connectivity matrices whose entries (links of the functional network) were weighted and directed. To render significant links, a z-score was introduced as $z = (u - \mu)/\sigma$, where u is a GTE value, μ is the average of all GTE values, and σ is their standard deviation. Those links that verified $z \geq z_{\text{th}}$, with $z_{\text{th}} = 2$, were deemed as significant and set to 1. The rest of the links were set to 0. The final functional network was thus directed and binarized. Postprocessing, analysis of GTE scores, and binarization were performed with Python scripts. The statistical properties of the inferred functional networks were also analyzed in Python using the Brain Connectivity Toolbox (BCT).[39] These properties include the distribution of connections, global efficiency G_{eff}, and community statistic Q. The global efficiency captures the capacity of the neuronal network to exchange information as a whole and varies between 0 (no communication) and 1 (full communication). The community statistic reflects the existence of functional microcircuits and varies between 0 (the whole network is the only functional circuit) and 1 (each single neuron is a functional microcircuit). The detailed description of these quantities and their use in the context of neuronal networks can be found in refs 32 and 40. Network plots were produced using the Python package *NetworkX*.[41]

Statistical Analysis. Immunohistochemistry experiments were performed in quadruplicate. Sixty scaffold samples from four similar independent culture experiments were used for immunocytochemical analysis at different culture time points using the combinations of different marker-specific antibodies. For quantification, the cells expressing progenitor, neuronal (quantification, Figure 1d: SOX2,

https://dx.doi.org/10.1021/acsami.0c16616
ACS Appl. Mater. Interfaces 2021, 13, 7839−7853

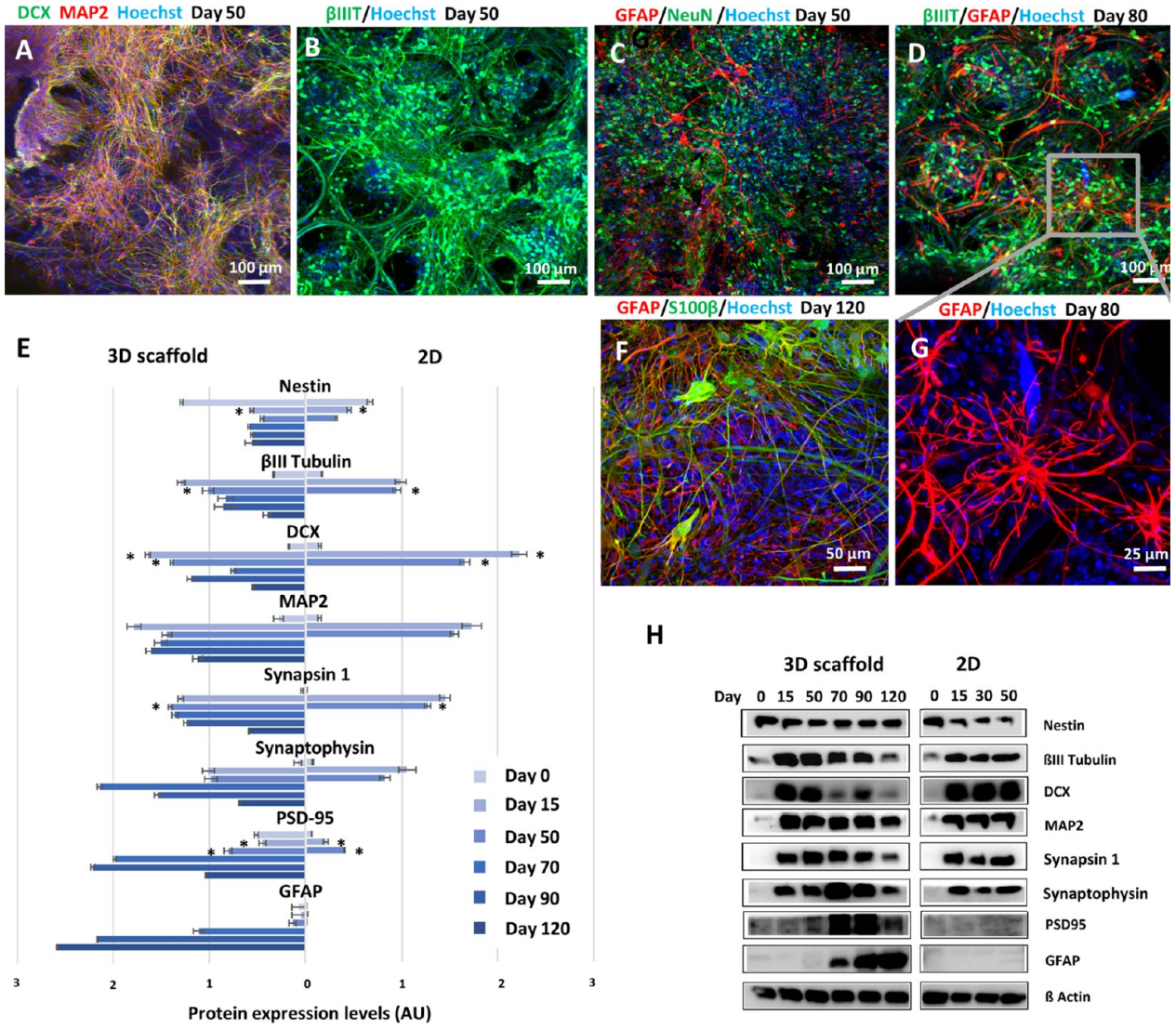

Figure 2. Neuronal network development on 3D scaffolds. (a–f) Representative images of the immunofluorescence analysis of neuronal and astrocyte markers over the course of neuronal differentiation. (a, b) At day 50, a well-developed neuronal network was characterized by a strong expression of MAP2 and *β*IIIT. (c, d) Astrocytes could be observed in the 3D culture after 50 days of differentiation, expanding their population along the 120 days of culture. (f, g) Representative images of astrocytes expressing either GFAP+ or S100*β*+, or cells co-expressing both astrocyte markers. (e, h) Western blot analysis of specific protein expression in 3D scaffold cultures compared to 2D control culture conditions. (g) Means ± SEM of respective protein. Data are normalized relative to *β*-actin band density and given in absolute units (AU) (n = 3). The significance difference between 2D and 3D conditions (at corresponding culture time point) was evaluated by the unpaired two-sample Student t test. *P < 0.05 was considered as a statistically significant difference.

DCX, and NeuN), and specific cortical neuronal markers (quantification, Figures 4f and 5i: GABA, vGLUT1, TBR1, CTIP2, FOXP2, BRN2, SATB2, and CUX1) were counted in every 10th layer of the LSM stack and estimated in percent relative to the total number of Hoechst 33342 positive cell nuclei. Data are presented as mean ± SEM. Statistical significance was evaluated using a paired two-tailed t test. *P < 0.5 was considered as a statistically significant difference.

For Western blot, protein expression analysis was performed twice for two independent culture experiments. The significant difference between 2D and 3D conditions (at corresponding culture time point) was evaluated by the unpaired two-sample Student t test. *P < 0.05 was considered as a statistically significant difference.

RESULTS AND DISCUSSION

Development of the Neuroglial Network on 2PP Fabricated 3D Scaffolds. A central aspect in scaffold-based neuronal networks is the material used for fabrication of the 3D structures, whose properties must ensure optimal laser-based scaffold fabrication together with successful and long-term *in vitro* network formation. These properties include biocompatibility, effective processability by a chosen laser source, long-term stability in culture, and low autofluorescence. We used DClear material, which is claimed as Class IIa long-term biocompatible resin, to fabricate 3D scaffold platforms.[29] Depending on the photoinitiator used for material composition, scaffolds fabricated from photopolymeric materials often exhibit high levels of autofluorescence[42] that substantially hinder, or totally mask, fluorescence-based image analysis.

DClear, the material of our choice, has a relatively low level of autofluorescence, which enables immunofluorescence analysis with all relevant protein bounding fluorophores and, more importantly, allows for the monitoring of neuronal

https://dx.doi.org/10.1021/acsami.0c16616
ACS Appl. Mater. Interfaces 2021, 13, 7839–7853

activity within the 3D scaffold through fluorescence calcium imaging.[43]

With the adequate material at hand, the 3D scaffold design of our choice consisted of three layers of hollow cylinder arrays (*honeycomb*, Figure 1a,b, Figure S1) that shaped an intricate architecture whose finest structure was given by the 30 μm thick cylinder's wall. The inner diameter of each cylinder in each layer was 240 μm. The entire scaffold structure was volumetrically permeable for cell infiltration and nutrient transport via culture media. The proposed 3D scaffold architecture consisting of the cylinder arrays has been previously successfully applied for the culturing of neuronal cells.[25] Such scaffold design allowed for the noninvasive high-resolution visualization of real-time cell growth and neuronal network formation in a 3D environment (Figure 1b). This permitted the rapid, label-free monitoring of culture health and represents an important benefit especially for long-term culture maintenance. To prevent possible lateral scaffold deformations during manipulation, culturing, and solvent-based development postprocessing, the honeycomb scaffold was strengthened by adding an outer ring structure of the same material. This polymeric ring border, together with two holes at its ends, also enabled a more accurate handling of the scaffold and the fragile neuronal networks forming on it.

Development of the Neuroglial Network on the 3D Scaffold. Immunofluorescence analysis revealed that the fabricated honeycomb scaffold provides a suitable 3D microniche for the quick maturation of NSCs, facilitating the formation and long-term viability of neuronal networks. 2D control cultures, consisting of neurons grown on a flat disk of DClear and cultured in identical conditions, could be maintained for up to 50 days. After that time, irreversible cell delamination began to occur.

We observed that NSCs colonized well the honeycomb structure, with the majority of cells attaching to the laminin-coated scaffold surface. Indeed, as revealed by immunofluorescence analysis with antibodies against Nestin and PAX6, once the scaffold was seeded with NSCs, the cells could uniformly accommodate within its pores and preserve cortical stem cell characteristics (Figure 1b,c). The method of cell expansion on scaffolds prior to differentiation also allowed cells to form colonies in the scaffold pores and to establish cell-to-cell contacts that are required for their better survival.[44]

We could observe typical ontogenic changes in the differentiation of NSCs within the scaffold, including the expansion phase, neurogenic phase, and gliogenic phase. After 4 weeks in culture, the developed network was uniformly distributed throughout the large scaffold area. Neuronal cells robustly expressed neuron-specific cytoskeletal and nuclear markers, including neuronal migration protein doublecortin (DCX), microtubule-associated protein 2 (MAP2), and neuronal nuclei (NeuN) (Figure 1e−g). The proportions of immature neurons, mature neurons, and neuronal progenitors were quantified, indicating that DCX+ young neurons constituted 37% of the overall cell population on the 3D scaffold, mature NeuN neurons 29%, and SOX2+ cortical progenitors the remaining 22% (Figure 1d). The early marker of neuronal identity DCX constantly decreased, giving rise to a more pronounced expression of beta III tubulin (βIIIT) and the mature neuronal marker MAP2. These MAP2-positive neurons also contained long neurites (Figures 1f and 2a). Notably, at day 25 of 3D culture, a large proportion of neurons already expressed the early-born cortical neuronal marker CTIP2 (Figure 1h).

To quantify and compare the gene and protein expression levels of several neuronal and glial markers, RT-PCR and Western blot analyses were performed at different time points of neuronal culturing. In accordance with the immunofluorescence analysis, we observed a high expression of neuronal markers DCX, MAP2, and βIIIT (Figure 2a,b,d,h). Notably, the DCX protein expression level was 9-fold higher at day 15 compared to the beginning of neuronal differentiation and was consistently downregulated after day 15. A persistent increase in the MAP2 protein expression levels (starting from day 15: 6-fold compared to day 0) over 120 days in 3D culture was observed. In contrast, Nestin expression was downregulated during 3D neuronal differentiation (Figure 2e,h).

Human iPSC-derived neuronal progenitors are capable of generating a diversity of neuronal cell types including different types of neurons and glial cells−astrocytes. Glial differentiation started to occur at around day 50 in 3D scaffold cultures, and the appearance of cells with an astrocytic phenotype was confirmed by the increased GFAP and S100β protein and mRNA expression (Figures 2c−h, Figures S2 and S3).

At day 50 in 3D cultures, the GFAP protein expression achieved a 2-fold expression level compared to day 0, constantly raising the level during the course of cultivation and reaching a 40-fold expression level at day 120. By comparison, the GFAP protein expression in 2D cultures was upregulated only by 0.5-fold at day 50 compared to day 0, a factor 4 lower than that in 3D cultures (Figure 2e,h).

A rich and well-interconnected neuronal network with NeuN- and βIIIT-positive neurons was also characterized by the presence of GFAP+ cells (Figure 2c,d, Video S1). We observed both GFAP/S100β+ cells and GFAP− but S100β+ cells (Figure 2f, Figure S3). The analysis of genes specifically expressed by glial cells also revealed an increase in their mRNA expression. Compared to S100β, the GFAP gene expression was more robustly pronounced starting from day 50 and reached a 3.5-fold increase by day 120 (Figure S2b). These findings are in agreement with our immunofluorescence analysis, where S100β was co-expressed with GFAP at day 50 but became more prominent at a later culture stage (Figure 2f, Video S2).

GFAP/S100β+ cells were present throughout the entire 3D network, and their population increased over the 120 days of 3D culture course. Figure 2d,f,g shows well-developed GFAP+ cells with a complex morphology and numerous processes forming a well-delineated bushy territory that overlaps with other GFAP+ cells and βIIIT+ neurons. It is well known that astrocytes control synapse formation and function and that they play a crucial role in the proper neural development.[45] In our 3D scaffold system, the GFAP+ cells were distributed throughout the entire scaffold and developed spontaneously according to the temporal specification of CNS cells and without the need for ciliary neurotrophic factor (CNTF), leukemia inhibitory factor (LIF), or serum, previously described as activators of astrocyte differentiation.[46] This finding demonstrates the ability of our 3D culture scaffold-based approach to support temporal specification during NSC differentiation, which is known to be dependent on intrinsic competence states, reflected by the transcription factor regulation and epigenetic modifications of differentiation-related genes.[47]

https://dx.doi.org/10.1021/acsami.0c16616
ACS Appl. Mater. Interfaces 2021, 13, 7839−7853

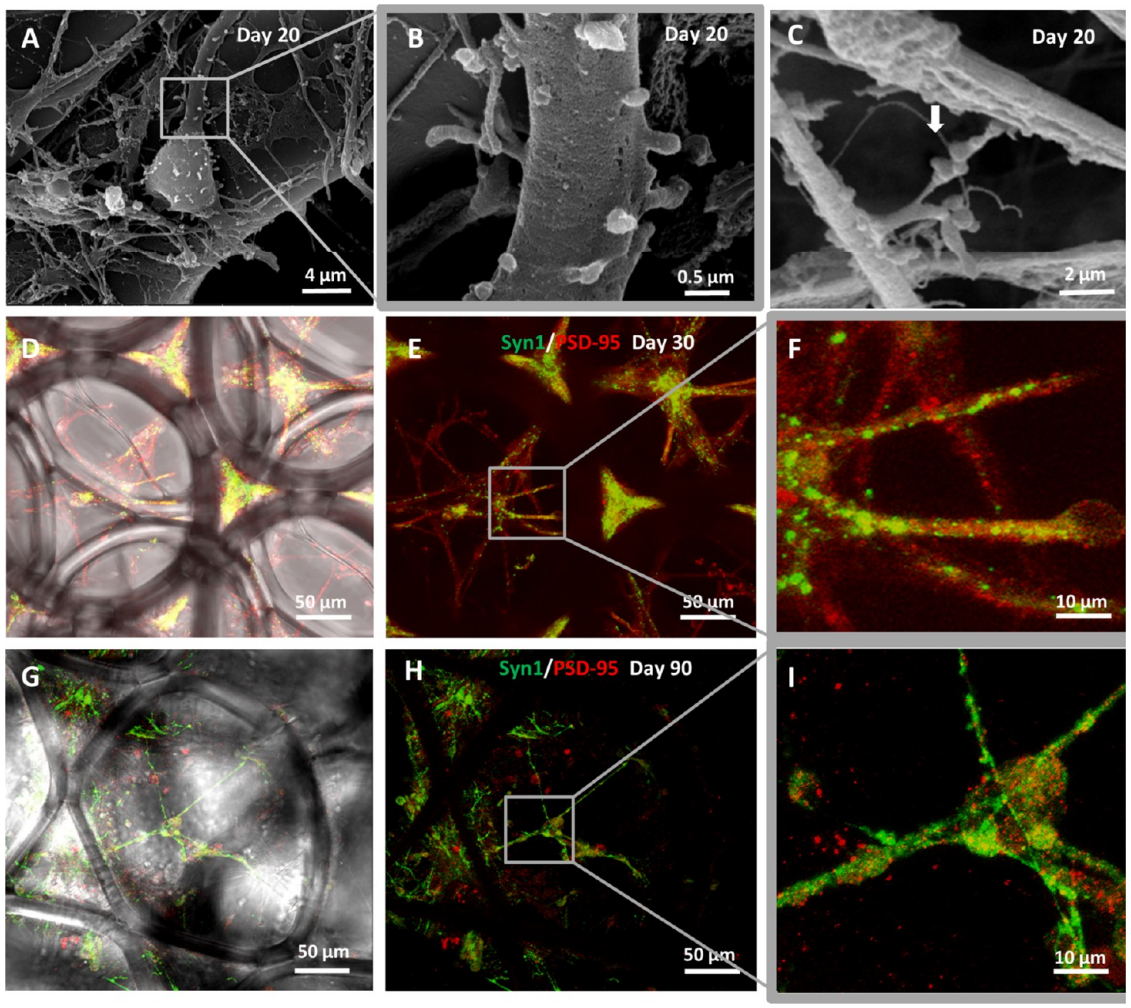

Figure 3. Formation of excitatory synapses in iPSC-derived cortical neurons on the 3D scaffold. (a–c) Scanning electron microscopy images of neurons at different magnifications. The arrow in (c) highlights dendritic spines and neuronal contacts formed by two neuronal cells at day 20 of differentiation. (d–i) Functional synapses were identified by immunofluorescence analysis of pre- and postsynaptic protein complexes through synapsin 1 or PSD-95 at day 30 (d–f) and at day 90 (g–i) of neuronal differentiation.

Synaptogenesis is a crucial step for neural network formation and function. Using our 3D scaffold-based culture system, we found that NSC-derived neurons start to form synapses at day 15 as confirmed by Western blot, RT-PCR, and electron microscopy analyses. Synapse formation occurred before the genesis of glial cells, which started to appear at around day 50. We examined the spine formation and synaptogenesis in the developing neuronal network using scanning electron microscopy and immunofluorescence analysis (Figure 3, Video S3). After 20 days of differentiation, a large number of cells exhibited the typical neuronal morphology with dendrites and axons spreading through many layers of other cell types of a more complex morphology. Typical dendritic spines were observed on day 20 of development (Figure 3a,b). Connections between neurons were also confirmed by the observation of physical spine contacts as indicated by the SEM analysis (Figure 3c, arrow). The formation of mature synapses on NSC-derived neurons was further examined using confocal microscopy and immunofluorescence analysis of pre- and postsynaptic proteins synapsin 1 and PSD-95, respectively. Their tight colocalization was observed starting from day 30 and further during the course of 3D culture and network development (Figure 3d–i). Moreover, as proved by calcium imaging, at day 25, the functionally active and connected network showed a strong activity with the presence of synchronous burst events (Video S4). Western blot and RT-PCR analysis of synaptophysin, synapsin 1 gene, and protein expression during the 120 day course of 3D culture showed that the gene expression of presynaptic markers synaptophysin and synapsin 1 was rather upregulated from the beginning of 3D network development (Figure 2e,h; starting from day 15; protein levels: synaptophysin, 13-fold and synapsin, 1–60-fold). Analysis of PSD-95 expression levels revealed a significant upregulation of mRNA and protein expression levels after 50 days of culture, when the MAP2 gene expression also reached 2- and 6-fold expression levels compared to day 0, respectively (Figure 2e,h, Figure S2).

Using immunofluorescence analysis, we found a mixed population of glutamatergic excitatory and GABAergic inhibitory neurons, while a previous study in NSC-derived neuronal networks in 2D conditions reported the generation of only glutamatergic neurons.[48] The glutamatergic projection neurons and GABAergic interneurons were generated within the developed network on 3D scaffold at day 50 (Figure 4a–e). The majority of neurons in the developed 3D network expressed the glutamate vesicular transporter vGLUT1,

https://dx.doi.org/10.1021/acsami.0c16616
ACS Appl. Mater. Interfaces 2021, 13, 7839–7853

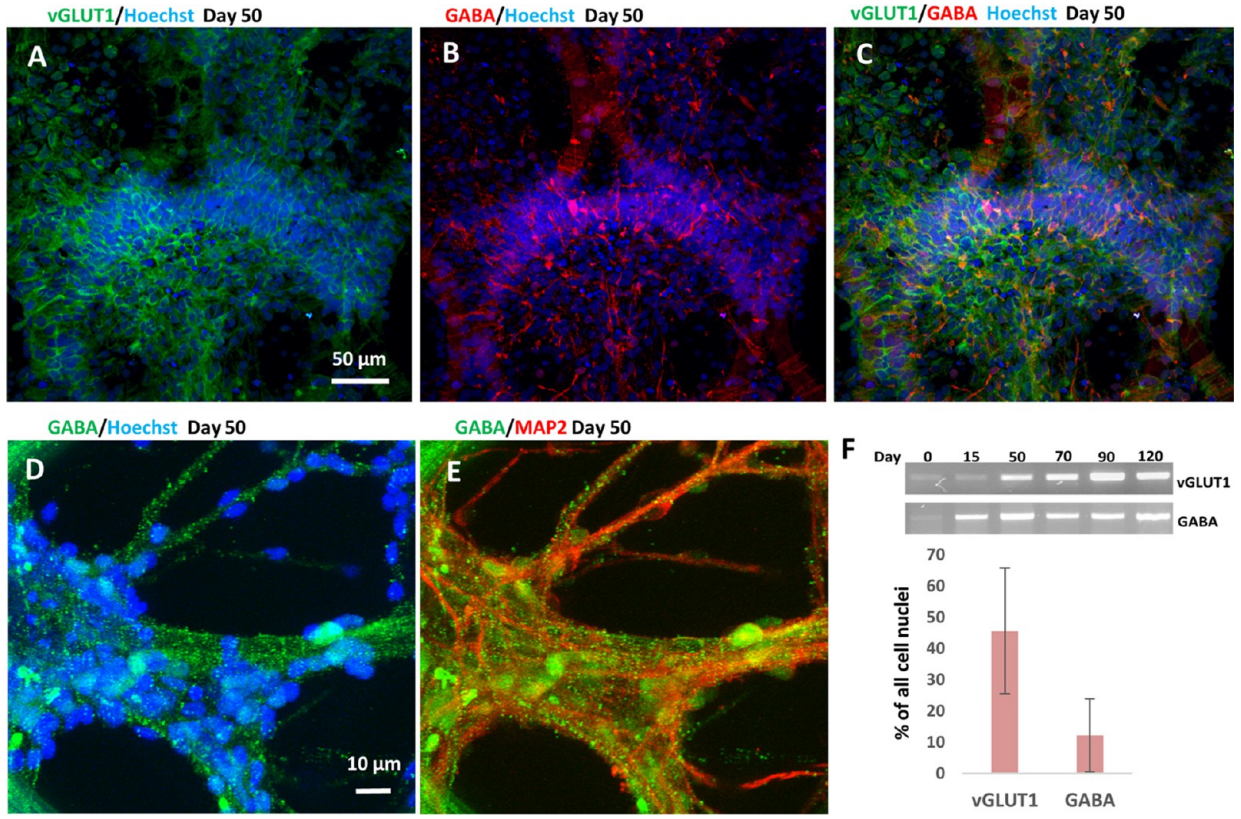

Figure 4. Characterization of excitatory and inhibitory neuronal subtypes in the 3D neuronal network. (a–e) Existence of specific excitatory vGLUT1+ and inhibitory GABA+ neuronal cells as revealed through immunofluorescence analysis. (f) Top panel shows the RT-PCR analysis of mRNA expression levels of vGLUT1 and GABA over the course of 120 days in culture. The bottom bar plot shows a quantification of the vGLUT1+ and GABA+ neuronal population in 3D culture at day 50. Data are shown as the percentage of vGLUT1+ and GABA+ neurons relative to all counted cell nuclei. Error bars are the standard error of the mean.

indicating that these cells are predominantly excitatory glutamatergic neurons. As assessed by quantification of the GABA+/vGLUT1+ ratio in the total neuronal population, the network was composed of about 45% excitatory glutamatergic neurons and 13% inhibitory GABAergic interneurons (quantified relative to the total counted amount of cell nuclei) (Figure 4c). By recalculation of this ratio within the GABA/vGLUT+ cell population, the proportion of GABA inhibitory neurons and vGLUT1 excitatory neurons constituted 22 and 78%, respectively. Notably, neither vGLUT1+ nor GABA+ cells could be detected with immunofluorescence analysis before day 50, although the mRNA analysis showed that the GABA expression level was moderately increased starting from the second week of culture (Figure 4f). vGLUT1 gene expression levels were not significantly upregulated in the beginning of 3D culture and up to day 50 of network development (Figure 4f). GABA+ interneurons are crucial to both the development and function of the cerebral cortex. The proportion of 22% of GABAergic interneurons on our 3D culture system is reflective of the known abundance of inhibitory neurons in both mouse and human brain tissues.[49] Hence, our results on 3D cultures are in line with the previously reported characterization of generation of glutamatergic and GABAergic neurons from iPSCs using 3D hydrogel and neurosphere culture methods, where similar proportions of GABAergic interneurons and glutamatergic projection neurons were reported.[50,51] Thus, it is evident that our engineered scaffold-based 3D neuronal culture generated from NSCs can recapitulate the naturally formed neuronal variability and does not require an extra addition of inhibitory interneurons.

Differentiation of Layer-Specific Cortical Excitatory Neurons in 3D Conditions. To assess whether the neurons expressed cortical layer specific markers, immunofluorescence quantification of a set of neuronal specific transcription factors was performed at days 50 and 120 of 3D network development (Figure 5). TBR1, CTIP2, FOXP2, BRN2, SATB2, and CUX1 are transcription factors that are expressed in each class of neurons according to the cortex layered temporal specification.[52,53] We found that the generation of cortical projection neurons from hiPSC-derived NSCs in our 3D scaffold system is similar to the earlier reported neurogenesis in 2D.[48] Deep- and upper-layer neurons were generated from NSCs in temporal order, starting from the generation of deep-layer neurons (CTIP, layer V-VI) already at day 25 of culture.

At day 50, TBR1 and CTIP2 neurons of the deep cortical layer (V–VI) were present in a large quantity (33 ± 6 and 44 ± 10% from counted cell nuclei, Figure 5i) and distributed over the entire 3D network (Figure 5,a,b). FOXP2 (layer V-VI)-positive neurons constituted 25 ± 1% and formed separate cellular clusters randomly located at different scaffold sites (Figure 5c). Of note, the upper-layer BRN2 gene was upregulated from the beginning of culture (Figure S2b); BRN2, as well as SATB2 neurons, could be first detected starting from day 50 of the network development (Figure 5c,d). These upper-layer cortical neurons were represented by 8 ± 2% of SATB2 neurons and 12 ± 2% of BRN2 neurons (Figure 5i). No CUX1-positive upper-layer neurons were

https://dx.doi.org/10.1021/acsami.0c16616
ACS Appl. Mater. Interfaces 2021, 13, 7839–7853

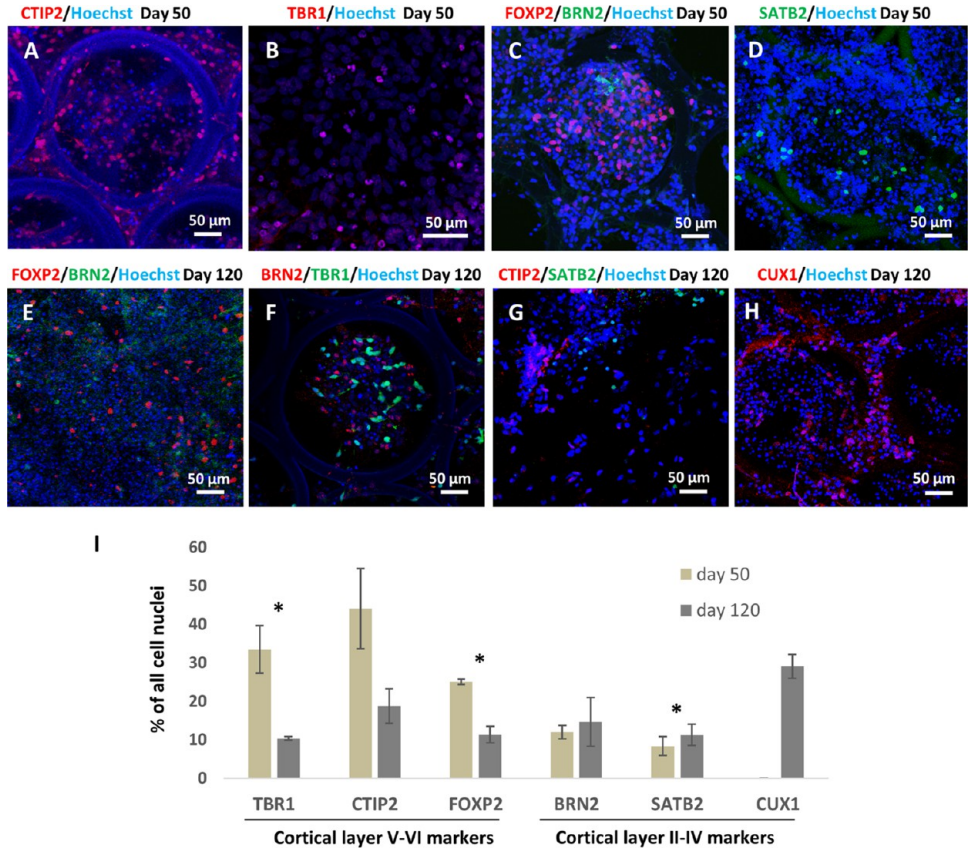

Figure 5. Differentiation of human cortical projection neurons on the 3D scaffold from neuronal progenitors at days 50 and 120. (a–d) Analysis of expression of lower and upper cortical neuron markers at day 50. In panels a and b, CTIP2+ and TBR1+ neurons are present in a large quantity and are evenly distributed over the entire scaffold structure. By contrast, in panels c and d, SATB2+, BRN2+, and FOXP2+ neuronal populations formed individual SATB2+, BRN2+, and FOXP2+ cell clusters randomly localized at different scaffold sites. (e–h) All types of cortical neurons were consistently distributed throughout the scaffold structure at day 120. (i) Relative proportions of different classes of cortical projection neurons at days 50 and 120. Error bars represent standard error of the mean. * indicates $P < 0.5$ significance (paired two-tailed Student's t test).

detected at day 50. By day 120 of neuronal network development, the number of TBR1, CTIP2, and FOXP2 neurons significantly decreased compared to day 50. In addition, TBR1 gene expression was significantly down-regulated starting from day 50 (Figure S2b). The proportions of BRN2 and SATB2 neurons slightly increased up to 14 ± 6 and 11 ± 3%, respectively, and these upper-layer neurons were distributed over the entire 3D culture volume. At day 120 of network development, 29 ± 3% of CUX1-positive deep cortical layer neurons could be quantified.

We observed a clear decrease in the proportion of cortical neuron of layers V–VI at day 120 of culture compared to day 50, as indicated by the quantitative analysis of cortical markers in these culture time points (Figure 5i). We ascribe the decrease to the processes of neurogenic to gliogenic transition and differentiation of additional neuronal subtypes.[47] Astrocytes started to appear in cultures at around day 50 and steadily increased their number over 120 days.

In terms of neuronal cell expansion, neuronal differentiation, and cortical specification, our 3D scaffold culture system demonstrated *in vivo* like neuronal tissue development during the long-term *in vitro* culture over 120 days.[54] In contrast, 2D control cultures, prepared as a flat layer of the same scaffold material and cultured identically, could be maintained only up to 50 days. After that, irreversible cell delamination began to occur. For this reason, the comparison of protein and gene expression levels between 2D and 3D cultures could be carried out only up to 50 (Figure S2, Western blot and RT-PCR analysis). This fact highlights the benefits of the developed 3D scaffold-based culture and emphasizes the importance of 3D cellular spatial arrangement for prolonged cellular survival.

Additionally, starting from day 50, we observed a notable population of OLIG2+ cellular nuclei, as well as occasional clusters of choline acetyltransferase expressing cells (ChAT+) and tyrosine hydroxylase (TH+) dopaminergic neurons (Figure S4). At day 50, large OLIG2+ nuclei were not clearly associated with the expression of neuronal MAP2 and βIIIT (Figure S4a,b). Hence, by performing the immunofluorescence analysis at day 120 of culture, we could confirm the presence of MAP2/OLIG2 co-expressing neuronal cells (Figure S4e). These cells can represent the population of corticospinal motor neurons in our 3D culture.[55] Corticospinal motor neurons are highly specialized long-distance projection neurons, and they represent an important component of the motor neuron circuitry.[56] Clusters of ChAT-expressing cells were detected at day 50 of culture, and by day 90, they were equally distributed within the developed neuronal network (Figure S4f,g; arrows indicate the clusters of ChAT+ cells). These cholinergic ChAT-positive neurons can constitute both motor neuron cell population and intrinsic cholinergic interneurons of the cortex. Cholinergic interneurons of the cortex have been reported to have a locally restricted modulatory effect on small cortical units and play a role in the increase of network activity in the cortex.[57] Cholinergic interneurons are an important neural cell

https://dx.doi.org/10.1021/acsami.0c16616
ACS Appl. Mater. Interfaces 2021, 13, 7839–7853

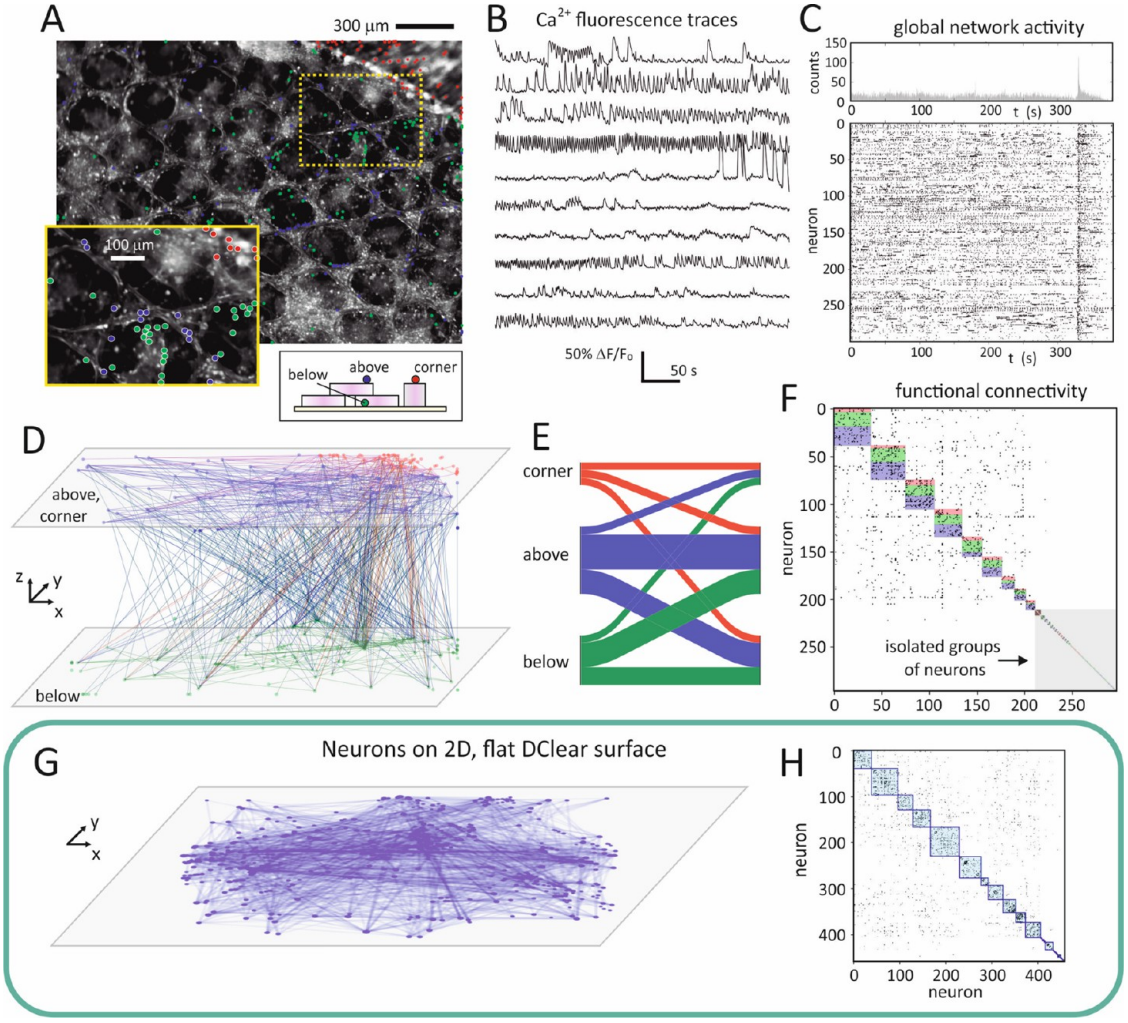

Figure 6. Analysis of calcium imaging data of neuronal networks grown and differentiated on the 3D scaffolds for 50 days (see Video S5 for visualization). (a) Fluorescence image showing ROI positions (neurons) as colored dots. Inset shows the enlarged area marked in yellow. The sketch at the bottom shows the color scheme used to classify neurons according to their position ("layer") in the scaffold. Red: top layer in the corner, blue: neurons on top of the scaffold, and green: neurons inside and below the scaffold. (b) Representative fluorescence traces of 10 neurons. Sharp peaks reveal activity. (c) Raster plot of spike times (bottom) and global network activity (top). A network burst occurs toward the end of the recording. (d) Graphical representation of the effective network with layers shifted vertically. Edges are colored according to the neuron from which they originate. (e) Flow diagram of connectivity between layers. (f) Effective connectivity matrix ordered by functional community. The color bars within each community indicate the proportion of neurons from each layer. (g) Effective connectivity of a control culture grown on a flat DClear surface. (h) Corresponding connectivity matrix with the communities highlighted.

type for certain pathological models. In Alzheimer's, for instance, the first type of neurons to degenerate is the acetylcholinergic neurons present in the nucleus basalis of Meynert.[58] The ability of our 3D cultures to support the formation of a distributed population of corticospinal neurons and cholinergic interneurons, among other cell types, represents a promising approach for the creation of *in vitro* model systems to study the onset and development of disease-related malfunctions and explore their treatment.

Functionality of Neuronal Networks in 3D Culture. The ability of NSCs to form a functionally active neuronal network was investigated through calcium fluorescence imaging. In these experiments, we compared Ca^{2+} activity of cells growing on honeycomb 3D scaffolds with standard cultures grown on a flat DClear surface (50 day old cultures, Figure 6 and Figure S5 for 2D data). Calcium imaging allowed the monitoring of spontaneous activity of about 300−500 neural cells (neurons and glia) in an area of 2.1 × 1.4 mm^2 (see corresponding Ca-imaging movie on Video S5). Although we did not the study the impact of astrocytes in dynamics and functional connectivity, it is known that astrocytes are important for orchestrating collective activity and facilitating neuronal synchronization.[59,60] Thus, the observed network bursts in the raster plot were most likely regulated by the astrocyte population. We observed that calcium traces of neurons and glia are different, with the former exhibiting a sharp increase upon activation followed by a slow decay and the latter exhibiting smooth variations. This difference, also observed by others, allowed us to discern both populations and, therefore, from here onward, we considered only the neuronal population to gain insight on the functionality of the neuronal network and its properties.[61,62]

Figure 6a shows a representative fluorescence image and the inferred regions of interest (ROIs) filtered out to highlight only neurons. The cells tended to aggregate along the scaffold structure, although individual cell bodies could be resolved

https://dx.doi.org/10.1021/acsami.0c16616
ACS Appl. Mater. Interfaces 2021, 13, 7839−7853

Table 1. Comparison of Effective Connectivity Traits between 2D and 3D Networks[a]

	connections per neuron, k	global efficiency, G_{eff}	community statistic, Q	number of communities (at least 5 neurons)	community size (at least 5 neurons)
2D, flat DClear	40 ± 12	0.42 ± 0.09	0.44 ± 0.03	12 ± 2	114 ± 17
3D, "honeycomb"	16 ± 7	0.26 ± 0.08	0.56 ± 0.04	7 ± 2	84 ± 9

[a]Each configuration is an average over 4 network realizations, recorded at day 50 and containing on the order of 500 neurons. Data are shown as the mean ± standard deviation of the mean. For the number of communities and their size, only groups containing five neurons or more were considered.

well. As shown at the bottom of Figure 6a, neurons were classified in three layer categories: neurons growing on top of the scaffold (in blue), those growing inside the scaffold (in green), and those growing in the bottom right corner that lies above the scaffold structure (in red).

Calcium imaging demonstrated that neurons were active in all layers, as illustrated by the representative fluorescence traces shown on Figure 6b, with sharp increases in amplitude relative to the baseline that revealed action potentials being elicited. Neurons displayed contrasting activity patterns, with some firing continuously with low amplitude and others firing scarcely but with high amplitude. Despite this variability, the network as a whole showed strong activity as illustrated in the raster plot of Figure 6c and with the presence of a synchronous event (network burst) by t = 330 s.

The network of connections between neurons was obtained using generalized transfer entropy (GTE), and significant connections were retained for analysis.[37,38] The map of connections is shown in Figure 6d, with the various layers offset vertically to highlight both intra- and interlayer connectivity. As the map of connections indicates that neurons connected richly within and between layers, we found it convenient to illustrate the degree of interconnectivity through an alluvial diagram (Figure 6e). Here, the "corner" layer connected equally with itself and other layers, the "above" layer connected preferentially to itself (50% of connections) and to "below" (40%), and the "below" layer mostly connected to "above" (50% of connections) and to itself (35%). However, in terms of the absolute number of connections, the "above" and "below" layers interconnected very similarly.

To further characterize the traits of the functional network, we analyzed the communities, i.e., groups of neurons that were more connected with themselves than with the rest of the network. To visually highlight these communities, the connectivity matrix was reordered by community size and layer using the Louvain modularity algorithm, with the modules appearing along the diagonal of the connectivity matrix. The analysis is shown in Figure 6f. Boxes indicate communities, and colored bands within them mark the layer to which neurons belong. We note that there were 11 communities containing more than 4 neurons and that all 3 layers were represented in each community. These communities were functionally linked to one another, as shown by the existence of abundant connections outside the communities. On average, a neuron connected with another nine, either within a community or with other neurons in the network. We also note that there were about 50 independent neurons in the network, i.e., neurons that were active but not connected to any other neuron.

To put the results of the scaffold network connectivity in comparative context, we next analyzed the functional traits of a 50 day old network grown on a flat DClear surface. As shown in Figure 6g, here all cells of the network belonged to a single layer, and effective connections extended the entire culture. The connectivity matrix of Figure 6h also showed abundant functional communities that were in general bigger and with much less isolated neurons than those in the 3D counterpart. The average connectivity in 2D was also larger, with about 17 connections per neuron on average. This comparison suggests that 3D networks tend to form smaller functional microcircuits that reflect a richer dynamic repertoire of the network. The details of the 2D experiment, including the representative traces and raster plot, are provided in Figure S5. The corresponding video of neuronal activity is shown in Video S6.

The comparison of the functional traits between the 3D scaffold and the 2D surface allows us to evaluate how the scaffold affects the connectivity between neurons. Compared to 2D, there is an indication that the scaffold favors connectivity at a local scale, with a tendency to shape microcircuits that translate into a relatively low number of connections and a larger number of functional communities. Thus, the functional connectivity derived from the calcium fluorescence can be seen as a proxy of the anatomical connectivity (i.e., synaptic links among neurons) at the scale of the whole network. While immunostaining revealed the presence of a remarkable number of astrocytes and formation of synaptic links in the pores of the scaffold, the functional connectivity informed about links among neurons only, which comprised both short- and long-range connections, shaping a network that can exchange information globally and exhibit collective activity events in the form of network bursts.

To show that the contrasting differences between the 2D and 3D configurations were reproducible among realizations, we extended the above analyses to four realizations in both networks and averaged the results. The networks in all cases were analyzed at day 50 and contained about 500 neurons. As shown in Table 1, the average results showed distinct features between configurations. Neurons in the 3D networks had fewer effective connections, which are expected since the presence of physical constraints reduces the capacity of neurons to find neighbors to connect to. The global efficiency G_{eff}, which captures the capacity of the neurons to communicate across the network, is lower in 3D, indicating that the neurons tend to communicate at a more local scale. The community statistic Q, which reflects the tendency of neurons to shape functional microcircuits, is larger in 3D than in 2D, indicating that the 3D architecture favors niches for microcircuits to form. This is strengthened by the observation that 3D cultures shape communities that are about 30% smaller than the 2D equivalent.

In line with these experimental observations, recent numerical simulations on neuronal networks grown in patterned substrates indicate that physical obstacles or scaffolds favor the emergence of microcircuits that translate into an abundance of functional communities.[40] The study also

https://dx.doi.org/10.1021/acsami.0c16616
ACS Appl. Mater. Interfaces 2021, 13, 7839−7853

showed that it was not possible to directly link the arrangement of the physical obstacles with the functional traits of the network except for the extreme case in which cell positioning and connectivity were strongly dictated. Thus, although the biological mechanisms that promote neuronal connectivity are complex, we would expect that the hollow cylinders in our 3D scaffold could promote strongly coupled microcircuits at the bottom layer, which would be weakly linked to other microcircuits through the top layer. However, the community analysis shows that the microcircuits are shaped by an approximately equal number of neurons belonging to the top and bottom layers. If the cylinders were higher, then we would expect that connections from the bottom layer to the top layer could be reduced or entirely removed. This is a difficult endeavor to test experimentally since extremely confined or isolated microcircuits may fail to form due to the lack of inputs and chemical sensing from other cells in the network, ultimately yielding a network that cannot survive.

Nevertheless, it is clear from our data that there appear overall features of the network distinguishing the 3D cultures formed in the scaffold from the 2D ones. The scaffold clearly induces changes in the way the neurons of the neuronal network connect to each other, defining an overall different functional organization, as also observed by others.[1] In terms of the geometry of the scaffold, it could be possible that the cylinders increase the local density of the cells, which in turn strengthens the communication among these neurons and their functional coupling in the form of communities. This is supported by recent experimental studies linking spatial aggregation and connectivity.[63] We may conclude that local connectivity appears to be strengthened by the presence of the 3D scaffold structure, although further explorations would be required to draw solid links between the geometric constraints and emerging functional traits. We believe that our capacity to reproducibly culture iPSC-derived neurons in tailored structures already paves the way toward future explorations with more complex and functional scaffold designs.

Applied laser fabrication technology allows the development of a scaffold device that will provide a means to electrically interrogate 3D *in vitro* cultures of electrically active cells, such as neurons, using integrated 3D microelectrodes−3D multi-electrode arrays (3D-MEA). Having a porous scaffold with an increased solid surface for cell attachment is more beneficial for the application of a pure hydrogel for the creation of 3D-MEA, as it lacks the problem of hydrogel lysis and allows the long-term culture and study of electrically active cells.[17,64] On the other hand, similar to the works of D. Kaplan's group, our scaffolds (with or without integrated electrodes) can certainly be combined with many types of tissue engineering relevant hydrogel to develop more complex organoid systems.[18,19,65]

CONCLUSIONS

Taken together, our laser-produced 3D scaffold-based system enabled the long-term culture of human iPSC-derived neuronal networks over 120 days. This long-term culture maintenance, therefore, facilitated iPSC-derived neuronal progenitors to develop into functional neuron−glia networks consisting of cortical projection neurons of all six cortical layers, different types of interneurons, and astrocytes. Calcium imaging allowed for the quantification of functional network connectivity, indicating that the scaffold structure promotes the development of local connectivity of neuronal circuits. The ability of NSCs to generate different types of neuronal cells, when grown on the 3D scaffold platform, enables future functional studies of the human cortex development. Our newly developed 3D culture approach represents a new platform with a high potential for the development of physiological *in vitro* models of human neuronal networks. Upon the development of reliable reprogramming and differentiation protocols for the generation of specific human neuronal subtypes, the comparative analysis and more focused investigations on disease modeling involving 3D scaffolds and selectively affected subtypes will become possible. Moreover, the proposed 3D scaffold-based culture system will not only allow new insights into *in vitro* modelling of neurological diseases with but also will enable the creation of engineered tissue constructs for studying innervation of different types of tissues, such as the skin, muscle, bone, and cornea.

ASSOCIATED CONTENT

Supporting Information

The Supporting Information is available free of charge at https://pubs.acs.org/doi/10.1021/acsami.0c16616.

NSC-derived network of neurons and astrocytes at day 80 (AVI)

Astrocyte network at day 120 (AVI)

Mature neuronal network at day 70 (AVI)

Calcium fluorescence imaging (3D) at day 25 (AVI)

Calcium fluorescence imaging (3D) at day 50 (AVI)

Calcium fluorescence imaging (2D) at day 50 (AVI)

CAD design of a 3D scaffolds and detailed cross section (Figure S1), Western blot and RT-PCR analyses (Figure S2), Astrogenesis in a 3D scaffold-based neuronal cultures at day 50 (Figure S3), Immunufluorescence characterisation of specific neuronal and glial cell populations (Figure S4), Fluorescence calcium imaging of a neuronal network grown in 2D conditions (Figure S5), list of RT-PCR and PCR oligonucleotide primers (Table S1), list of antibodies used for immunostaining and Western blotting (Table S2) (PDF)

AUTHOR INFORMATION

Corresponding Author

Anastasia Koroleva − *Institute of Quantum Optics, Leibniz University Hannover, 30167 Hannover, Germany; Institute for Regenerative Medicine, Sechenov University, 119991 Moscow, Russia; Laser Zentrum Hannover e.V., 30419 Hannover, Germany;* orcid.org/0000-0003-1937-1031; Email: koroleva@iqo.uni-hannover.de

Authors

Andrea Deiwick − *Institute of Quantum Optics, Leibniz University Hannover, 30167 Hannover, Germany*

Ayman El-Tamer − *Laser Zentrum Hannover e.V., 30419 Hannover, Germany*

Lothar Koch − *Institute of Quantum Optics, Leibniz University Hannover, 30167 Hannover, Germany*

Yichen Shi − *Axol Bioscience Ltd., CB10 1XL Cambridge, UK*

Estefanía Estévez-Priego − *Departament de Física de la Matèria Condensada, Universitat de Barcelona, 08028 Barcelona, Spain; Universitat de Barcelona Institute of Complex Systems (UBICS), 08028 Barcelona, Spain*

Adriaan-Alexander Ludl − *Departament de Física de la Matèria Condensada, Universitat de Barcelona, 08028*

https://dx.doi.org/10.1021/acsami.0c16616
ACS Appl. Mater. Interfaces 2021, 13, 7839−7853

Barcelona, Spain; Universitat de Barcelona Institute of Complex Systems (UBICS), 08028 Barcelona, Spain; Computational Biology Unit, Department of Informatics, University of Bergen, 5020 Bergen, Norway

Jordi Soriano − *Departament de Física de la Matèria Condensada, Universitat de Barcelona, 08028 Barcelona, Spain; Universitat de Barcelona Institute of Complex Systems (UBICS), 08028 Barcelona, Spain*

Daria Guseva − *Cellular Neurophysiology, Hannover Medical School, 30625 Hannover, Germany; Department of Nutritional Medicine, University of Hohenheim, 70599 Stuttgart, Germany*

Evgeni Ponimaskin − *Cellular Neurophysiology, Hannover Medical School, 30625 Hannover, Germany*

Boris Chichkov − *Institute of Quantum Optics, Leibniz University Hannover, 30167 Hannover, Germany*

Complete contact information is available at: https://pubs.acs.org/10.1021/acsami.0c16616

Author Contributions

△A.K. and A.D. contributed equally.The manuscript was written through contributions of all authors. All authors have given approval to the final version of the manuscript.

Notes

The authors declare no competing financial interest.

■ ACKNOWLEDGMENTS

This work was funded by European Union's Horizon 2020 projects MESO-BRAIN, Grant 713140, and'Scaffold Needs', Grant 851734. This work was supported by Deutsche Forschungsgemeinschaft through Grant PO732 and Excellence Cluster REBIRTH (E.P.), and through Grant GU1521/4-1 (D.G.). A.K. acknowledges Grant 19-75-10008 (2PP scaffold characterization) from Russian Science Foundation. J.S. also acknowledges the support from the Ministerio de Ciencia e Innovación (Spain), grants FIS2016-78507-C2-2-P and PID2019-108842GB-C21, and to the Generalitat de Catalunya, grant 2017SGR1061.

■ ABBREVIATIONS

2PP, two-photon polymerization
3D, three-dimensional
2D, two-dimensional
hiPSCs, human induced pluripotent stem cells
NSCs, neural stem cells
ICC, immunocytochemical

■ REFERENCES

(1) Dingle, Y. T. L.; Liaudanskaya, V.; Finnegan, L. T.; Berlind, K. C.; Mizzoni, C.; Georgakoudi, I.; Nieland, T. J. F.; Kaplan, D. L. Functional Characterization of Three-Dimensional Cortical Cultures for In Vitro Modeling of Brain Networks. *iScience* **2020**, *23*, 101434.

(2) Zhuang, P.; Sun, A. X.; An, J.; Chua, C. K.; Chew, S. Y. 3D Neural Tissue Models: From Spheroids to Bioprinting. *Biomaterials* **2018**, *154*, 113−133.

(3) Vanderburgh, J.; Sterling, J. A.; Guelcher, S. A. 3D Printing of Tissue Engineered Constructs for In Vitro Modeling of Disease Progression and Drug Screening. *Ann. Biomed. Eng.* **2017**, *45*, 164−179.

(4) Gilmour, A.; Poole-Warren, L.; Green, R. A. An Improved in Vitro Model of Cortical Tissue. *Front. Neurosci.* **2019**, *13*, 1−15.

(5) Enright, H. A.; Lam, D.; Sebastian, A.; Sales, A. P.; Cadena, J.; Hum, N. R.; Osburn, J. J.; Peters, S. K. G.; Petkus, B.; Soscia, D. A.; Kulp, K. S.; Loots, G. G.; Wheeler, E. K.; Fischer, N. O. Functional and Transcriptional Characterization of Complex Neuronal Co-Cultures. *Sci. Rep.* **2020**, *10*, 11007.

(6) Pagan-Diaz, G. J.; Ramos-Cruz, K. P.; Sam, R.; Kandel, M. E.; Aydin, O.; Saif, M. T. A.; Popescu, G.; Bashir, R. Engineering Geometrical 3-Dimensional Untethered in Vitro Neural Tissue Mimic. *Proc. Natl. Acad. Sci. U. S. A.* **2019**, *116*, 25932−25940.

(7) Shi, Y.; Kirwan, P.; Livesey, F. J. Directed Differentiation of Human Pluripotent Stem Cells to Cerebral Cortex Neurons and Neural Networks. *Nat. Protoc.* **2012**, *7*, 1836−1846.

(8) Lindvall, O.; Kokaia, Z. Stem Cells in Human Neurodegenerative Disorders — Time for Clinical Translation? *J. Clin. Invest.* **2010**, *120*, 29−40.

(9) Takahashi, K.; Tanabe, K.; Ohnuki, M.; Narita, M.; Ichisaka, T.; Tomoda, K.; Yamanaka, S. Induction of Pluripotent Stem Cells from Adult Human Fibroblasts by Defined Factors. *Cell* **2007**, *131*, 861−872.

(10) Frega, M.; Tedesco, M.; Massobrio, P.; Pesce, M.; Martinoia, S. Network Dynamics of 3D Engineered Neuronal Cultures: A New Experimental Model for in-Vitro Electrophysiology. *Sci. Rep.* **2014**, *4*, 1−14.

(11) Subia, B.; Rao, R. R.; Kundu, S. C. Silk 3D Matrices Incorporating Human Neural Progenitor Cells for Neural Tissue Engineering Applications. *Polym. J.* **2015**, *47*, 819−825.

(12) Shin, J.; Choi, E. J.; Cho, J. H.; Cho, A. N.; Jin, Y.; Yang, K.; Song, C.; Cho, S. W. Three-Dimensional Electroconductive Hyaluronic Acid Hydrogels Incorporated with Carbon Nanotubes and Polypyrrole by Catechol-Mediated Dispersion Enhance Neurogenesis of Human Neural Stem Cells. *Biomacromolecules* **2017**, *18*, 3060−3072.

(13) Li, H.; Wijekoon, A.; Leipzig, N. D. 3D Differentiation of Neural Stem Cells in Macroporous Photopolymerizable Hydrogel Scaffolds. *PLoS One* **2012**, *7*, No. e48824.

(14) Choi, S. H.; Kim, Y. H.; Hebisch, M.; Sliwinski, C.; Lee, S.; D'Avanzo, C.; Chen, H.; Hooli, B.; Asselin, C.; Muffat, J.; Klee, J. B.; Zhang, C.; Wainger, B. J.; Peitz, M.; Kovacs, D. M.; Woolf, C. J.; Wagner, S. L.; Tanzi, R. E.; Kim, D. Y. A Three-Dimensional Human Neural Cell Culture Model of Alzheimer's Disease. *Nature* **2014**, *515*, 274−278.

(15) Turunen, S.; Joki, T.; Hiltunen, M. L.; Ihalainen, T. O.; Narkilahti, S.; Kellomäki, M. Direct Laser Writing of Tubular Microtowers for 3D Culture of Human Pluripotent Stem Cell-Derived Neuronal Cells. *ACS Appl. Mater. Interfaces* **2017**, *9*, 25717−25730.

(16) Jakobsson, A.; Ottosson, M.; Zalis, M. C.; O'Carroll, D.; Johansson, U. E.; Johansson, F. Three-Dimensional Functional Human Neuronal Networks in Uncompressed Low-Density Electrospun Fiber Scaffolds. *Nanomed. Nanotechnol., Biol. Med.* **2017**, *13*, 1563−1573.

(17) Lam, D.; Enright, H. A.; Peters, S. K. G.; Moya, M. L.; Soscia, D. A.; Cadena, J.; Alvarado, J. A.; Kulp, K. S.; Wheeler, E. K.; Fischer, N. O. Optimizing Cell Encapsulation Condition in ECM-Collagen I Hydrogels to Support 3D Neuronal Cultures. *J. Neurosci. Methods* **2020**, *329*, 108460.

(18) Tang-Schomer, M. D.; White, J. D.; Tien, L. W.; Schmitt, L. I.; Valentin, T. M.; Graziano, D. J.; Hopkins, A. M.; Omenetto, F. G.; Haydon, P. G.; Kaplan, D. L. Bioengineered Functional Brain-like Cortical Tissue. *Proc. Natl. Acad. Sci. U. S. A.* **2014**, *111*, 13811−13816.

(19) Rouleau, N.; Cantley, W. L.; Liaudanskaya, V.; Berk, A.; Du, C.; Rusk, W.; Peirent, E.; Koester, C.; Nieland, T. J. F.; Kaplan, D. L. A Long-Living Bioengineered Neural Tissue Platform to Study Neurodegeneration. *Macromol. Biosci.* **2020**, *20*, 2000004.

(20) Song, J.; Michas, C.; Chen, C. S.; White, A. E.; Grinstaff, M. W. From Simple to Architecturally Complex Hydrogel Scaffolds for Cell and Tissue Engineering Applications: Opportunities Presented by Two-Photon Polymerization. *Adv. Healthcare Mater.* **2020**, *9*, 1−13.

(21) Gittard, S. D.; Koroleva, A.; Nguyen, A.; Fadeeva, E.; Gaidukeviciute, A.; Schlie, S.; Narayan, R. J.; Chichkov, B. Two-

Photon Polymerization Microstructuring in Regenerative Medicine. *Front. Biosci.* **2013**, *E5*, 602−609.
(22) Raimondi, M. T.; Eaton, S. M.; Laganà, M.; Aprile, V.; Nava, M. M.; Cerullo, G.; Osellame, R. Three-Dimensional Structural Niches Engineered via Two-Photon Laser Polymerization Promote Stem Cell Homing. *Acta Biomater.* **2013**, *9*, 4579−4584.
(23) Koroleva, A.; Deiwick, A.; Nguyen, A.; Schlie-Wolter, S.; Narayan, R.; Timashev, P.; Popov, V.; Bagratashvili, V.; Chichkov, B. Osteogenic Differentiation of Human Mesenchymal Stem Cells in 3-D Zr-Si Organic-Inorganic Scaffolds Produced by Two-Photon Polymerization Technique. *PLoS One* **2015**, *10*, No. e0118164.
(24) Kuznetsova, D.; Ageykin, A.; Koroleva, A.; Deiwick, A.; Shpichka, A.; Solovieva, A.; Kostjuk, S.; Meleshina, A.; Rodimova, S.; Akovanceva, A.; Butnaru, D.; Frolova, A.; Zagaynova, E.; Chichkov, B.; Bagratashvili, V.; Timashev, P. Surface Micromorphology of Cross-Linked Tetrafunctional Polylactide Scaffolds Inducing Vessel Growth and Bone Formation. *Biofabrication* **2017**, *9*, 025009.
(25) Timashev, P.; Kuznetsova, D.; Koroleva, A.; Prodanets, N.; Deiwick, A.; Piskun, Y.; Bardakova, K.; Dzhoyashvili, N.; Kostjuk, S.; Zagaynova, E.; Rochev, Y.; Chichkov, B.; Bagratashvili, V. Novel Biodegradable Star-Shaped Polylactide Scaffolds for Bone Regeneration Fabricated by Two-Photon Polymerization. *Nanomedicine* **2016**, *11*, 1041.
(26) Timashev, P. S.; Vedunova, M. V.; Guseva, D.; Ponimaskin, E.; Deiwick, A.; Mishchenko, T. A.; Mitroshina, E. V.; Koroleva, A. V.; Pimashkin, A. S.; Mukhina, I. V.; Panchenko, V. Y.; Chichkov, B. N.; Bagratashvili, V. N. 3D *in Vitro* Platform Produced by Two-Photon Polymerization for the Analysis of Neural Network Formation and Function. *Biomed. Phys. Eng. Express* **2016**, *2*, No. 035001.
(27) Timashev, P. S.; Bardakova, K. N.; Minaev, N. V.; Demina, T. S.; Mishchenko, T. A.; Mitroshina, E. V.; Akovantseva, A. A.; Koroleva, A. V.; Asyutin, D. S.; Pimenova, L. F.; Konovalov, N. A.; Akopova, T. A.; Solov'eva, A. B.; Mukhina, I. V.; Vedunova, M. V.; Chichkov, B. N.; Bagratashvili, V. N. Compatibility of Cells of the Nervous System with Structured Biodegradable Chitosan-Based Hydrogel Matrices. *Appl. Biochem. Microbiol.* **2016**, *52*, 508.
(28) Balyabin, A. V.; Tikhobrazova, O. P.; Muravyeva, M. S.; Klyuev, E. A.; Ponyatovskaya, A. V.; Shirokova, O. M.; Bardakova, K. N.; Minaev, N. V.; Koroleva, A. V.; Mitaeva, Y. I.; Mitroshina, E. V.; Vedunova, M. V.; Rochev, Y. A.; Chichkov, B. N.; Timashev, P. S.; Bagratashvili, V. N.; Mukhina, I. V. Long-Term Neurological and Behavioral Results of Biodegradable Scaffold Implantation in Mice Brain. *Sovrem. Tehnol. Med.* **2016**, *8*, 198.
(29) Moreno-Rivas, O.; Hernández-Velázquez, D.; Piazza, V.; Marquez, S. Rapid Prototyping of Microfluidic Devices by SL 3D Printing and Their Biocompatibility Study for Cell Culturing. *Mater. Today Proc.* **2019**, *13*, 436−445.
(30) Formlabs. *Dental LT Clear Safety Data Sheet* **2018**, *1*, 0.
(31) Orlandi, J. G.; Fernández-García, S.; Comella-Bolla, A.; Masana, M.; Barriga, G. G.-D.; Yaghoubi, M.; Kipp, A.; Canals, J. M.; Colicos, M. A.; Davidsen, J.; Alberch, J.; Soriano, J. NETCAL: An Interactive Platform for Large-Scale, NETwork and Population Dynamics Analysis of CALcium Imaging Recordings. *Neuroscience* **2017**, DOI: 10.5281/ZENODO.1119026.
(32) Fernández-García, S.; Orlandi, J. G.; García-Díaz Barriga, G. A.; Rodríguez, M. J.; Masana, M.; Soriano, J.; Alberch, J. Deficits in Coordinated Neuronal Activity and Network Topology Are Striatal Hallmarks in Huntington's Disease. *BMC Biol.* **2020**, *18*, 58.
(33) Schindelin, J.; Arganda-Carreras, I.; Frise, E.; Kaynig, V.; Longair, M.; Pietzsch, T.; Preibisch, S.; Rueden, C.; Saalfeld, S.; Schmid, B.; Tinevez, J. Y.; White, D. J.; Hartenstein, V.; Eliceiri, K.; Tomancak, P.; Cardona, A. Fiji: An Open-Source Platform for Biological-Image Analysis. *Nat. Methods* **2012**, *9*, 676−682.
(34) Van Der Walt, S.; Schönberger, J. L.; Nunez-Iglesias, J.; Boulogne, F.; Warner, J. D.; Yager, N.; Gouillart, E.; Yu, T.; scikit-image contributors. Scikit-Image: Image Processing in Python. *PeerJ* **2014**, *2*, 1−18.
(35) Friedrich, J.; Zhou, P.; Paninski, L. Fast Online Deconvolution of Calcium Imaging Data. *Acta Med. Okayama* **2017**, *13*, e1005423.
(36) Schreiber, T. Measuring Information Transfer. *Phys. Rev. Lett.* **2000**, *85*, 461−464.
(37) Stetter, O.; Battaglia, D.; Soriano, J.; Geisel, T. Model-Free Reconstruction of Excitatory Neuronal Connectivity from Calcium Imaging Signals. *PLoS Comput. Biol.* **2012**, *8*, No. e1002653.
(38) Orlandi, J. G.; Stetter, O.; Soriano, J.; Geisel, T.; Battaglia, D. Transfer Entropy Reconstruction and Labeling of Neuronal Connections from Simulated Calcium Imaging. *PLoS One* **2014**, *9*, No. e98842.
(39) Rubinov, M.; Sporns, O. Complex Network Measures of Brain Connectivity: Uses and Interpretations. *Neuroimage* **2010**, *52*, 1059−1069.
(40) Ludl, A.-A.; Soriano, J. Impact of Physical Obstacles on the Structural and Effective Connectivity of in Silico Neuronal Circuits. *Front. Comput. Neurosci.* **2020**, *14*, article 77, DOI: 10.3389/fncom.2020.00077.
(41) Hagberg, A. A.; Schult, D. A.; Swart, P. J. Exploring Network Structure, Dynamics, and Function Using NetworkX. In *7th Python in Science Conference (SciPy 2008)*; LANL, 2008; pp. 11−15.
(42) Crowe, J. A.; el Tamer, A.; Nagel, D.; Koroleva, A. V.; Madrid-Wolff, J.; Olarte, O. E.; Sokolovsky, S.; Priego-Estevez, E.; Ludl, A.; Soriano, J.; Chichkov, B. N.; Hill, E. J.; Parri, H. R.; Rafailov, E. U. Development of Two-Photon Polymerised Scaffolds for Optical Interrogation and Neurite Guidance of Human IPSC-Derived Cortical Neuronal Networks. *Lab Chip* **2020**, 1792.
(43) Grienberger, C.; Konnerth, A. Imaging Calcium in Neurons. *Neuron* **2012**, *73*, 862−885.
(44) Dong, J.; Pan, Y.-B.; Wu, X.-R.; He, L.-N.; Liu, X.-D.; Feng, D.-F.; Xu, T.-L.; Sun, S.; Xu, N.-J. A Neuronal Molecular Switch through Cell-Cell Contact That Regulates Quiescent Neural Stem Cells. *Sci. Adv.* **2020**, *5*, No. eaav4416.
(45) Ullian, E. M.; et al. Control of synapse number by glia. *Science* **2001**, *291*, 657−661.
(46) Okano, H.; Temple, S. Cell Types to Order: Temporal Specification of CNS Stem Cells. *Curr. Opin. Neurobiol.* **2009**, *19*, 112−119.
(47) Miller, F. D.; Gauthier, A. S. Timing Is Everything : Making Neurons versus Glia in the Developing Cortex. *Neuron* **2007**, *54*, 357−369.
(48) Shi, Y.; Kirwan, P.; Smith, J.; Robinson, H. P. C.; Livesey, F. J. Human Cerebral Cortex Development from Pluripotent Stem Cells to Functional Excitatory Synapses. *Nat. Neurosci.* **2012**, *15*, 477−486.
(49) Wonders, C. P.; Anderson, S. A. The Origin and Specification of Cortical Interneurons. *Nat. Rev. Neurosci.* **2006**, *7*, 687−696.
(50) Tekin, H.; Simmons, S.; Cummings, B.; Gao, L.; Adiconis, X.; Hession, C. C.; Ghoshal, A.; Dionne, D.; Choudhury, S. R.; Yesilyurt, V.; Sanjana, N. E.; Shi, X.; Lu, C.; Heidenreich, M.; Pan, J. Q.; Levin, J. Z.; Zhang, F. Effects of 3D Culturing Conditions on the Transcriptomic Profile of Stem-Cell-Derived Neurons. *Nat. Biomed. Eng.* **2018**, *2*, 540−554.
(51) Floruta, C. M.; Du, R.; Kang, H.; Stein, J. L.; Weick, J. P. Default Patterning Produces Pan-Cortical Glutamatergic and CGE/LGE-like GABAergic Neurons from Human Pluripotent Stem Cells. *Stem Cell Rep.* **2017**, *9*, 1463−1476.
(52) Molyneaux, B. J.; Arlotta, P.; Menezes, J. R. L.; Macklis, J. D. Neuronal Subtype Specification in the Cerebral Cortex. *Nat. Rev. Neurosci.* **2007**, *8*, 427−437.
(53) Alcamo, E. A.; Chirivella, L.; Dautzenberg, M.; Dobreva, G.; Fariñas, I.; Grosschedl, R.; McConnell, S. K. Satb2 Regulates Callosal Projection Neuron Identity in the Developing Cerebral Cortex. *Neuron* **2008**, *57*, 364−377.
(54) Caviness, V. S., Jr.; Takahashi, T.; Nowakowski, R. S. Numbers, Time and Neocortical Neuronogenesis: A General Developmental and Evolutionary Model. *Trends Neurosci.* **1995**, *18*, 379−383.
(55) Hu, B. Y.; Weick, J. P.; Yu, J.; Ma, L. X.; Zhang, X. Q.; Thomson, J. A.; Zhang, S. C. Neural Differentiation of Human Induced Pluripotent Stem Cells Follows Developmental Principles but with Variable Potency. *Proc. Natl. Acad. Sci. U. S. A.* **2010**, *107*, 4335−4340.

(56) Jara, J. H.; Stanford, M. J.; Zhu, Y.; Tu, M.; Hauswirth, W. W.; Bohn, M. C.; Devries, S. H.; Özdinler, P. H. Healthy and Diseased Corticospinal Motor Neurons Are Selectively Transduced upon Direct AAV2-2 Injection into the Motor Cortex. *Gene Ther.* **2016**, *23*, 272−282.
(57) Von Engelhardt, J.; Eliava, M.; Meyer, A. H.; Rozov, A.; Monyer, H. Functional Characterization of Intrinsic Cholinergic Interneurons in the Cortex. *J. Neurosci.* **2007**, *27*, 5633−5642.
(58) Ferreira-vieira, T. H.; Guimaraes, I. M.; Silva, F. R.; Ribeiro, F. M. Alzheimer's Disease: Targeting the Cholinergic System. *Curr. neuropharmacol.* **2016**, 101−115.
(59) Kiyoshi, C. M.; Zhou, M. Astrocyte Syncytium: A Functional Reticular System in the Brain. *Neural Regen. Res.* **2019**, *14*, 595−596.
(60) Pirttimaki, T. M.; Sims, R. E.; Saunders, G.; Antonio, S. A.; Codadu, N. K.; Parri, H. R. Astrocyte-Mediated Neuronal Synchronization Properties Revealed by False Gliotransmitter Release. *J. Neurosci.* **2017**, *37*, 9859−9870.
(61) Dawitz, J.; Kroon, T.; Hjorth, J. J. J.; Meredith, R. M. Functional Calcium Imaging in Developing Cortical Networks. *J. Visualized Exp.* **2011**, 1−8.
(62) Schnell, C.; Fresemann, J.; Hülsmann, S. Determinants of Functional Coupling between Astrocytes and Respiratory Neurons in the Pre-Bötzinger Complex. *PLoS One* **2011**, *6*, e26309.
(63) Tibau, E.; Ludl, A. A.; Rudiger, S.; Orlandi, J. G.; Soriano, J. Neuronal Spatial Arrangement Shapes Effective Connectivity Traits of in Vitro Cortical Networks. *IEEE Trans. Netw. Sci. Eng.* **2020**, *7*, 435−448.
(64) Soscia, D. A.; Lam, D.; Tooker, A. C.; Enright, H. A.; Triplett, M.; Karande, P.; Peters, S. K. G.; Sales, A. P.; Wheeler, E. K.; Fischer, N. O. A Flexible 3-Dimensional Microelectrode Array for: In Vitro Brain Models. *Lab Chip* **2020**, *20*, 901−911.
(65) Chwalek, K.; Tang-Schomer, M. D.; Omenetto, F. G.; Kaplan, D. L. In Vitro Bioengineered Model of Cortical Brain Tissue. *Nat. Protoc.* **2015**, *10*, 1362−1373.

https://dx.doi.org/10.1021/acsami.0c16616
ACS Appl. Mater. Interfaces 2021, 13, 7839−7853